Highlights

Causal Preconditioning Filters Design for Real-Time Multichannel Active Noise Control

Yiming Wang, Yongjie Zhuang, Yangfan Liu

- A causal preconditioning method is proposed for multichannel active noise control using spectral factorization and Riccati-based decomposition.
- The approach improves convergence speed and noise reduction performance without introducing additional delay, enabling real-time implementation.
- The method is validated through experimentally measured secondary paths, demonstrating its effectiveness in complex scenarios.

This manuscript was published in Applied Acoustics.

DOI: https://doi.org/10.1016/j.apacoust.2025.110950

Causal Preconditioning Filters Design for Real-Time Multichannel Active Noise Control

Yiming Wang[a,b], Yongjie Zhuang[c,1], Yangfan Liu[a,*]

[a]*Ray W. Herrick Laboratories, School of Mechanical Engineering, Purdue University, 177 S. Russell Street, West Lafayette, 47907, Indiana, USA*
[b]*AncSonic, Rm. 801, Building D3, Kexing Science Park, Nanshan District, Shenzhen, 518000, Guangdong Province, China*
[c]*Amazon Web Services, 2201 6th Ave, Seattle, 98121, Washington, USA*

Abstract

The least-mean-square (LMS) algorithm is widely used in active noise control (ANC) systems due to its simplicity and adaptability. However, in multichannel broadband applications, its convergence rate is often limited by correlations among reference signals and coupling within the secondary path responses. Previous efforts to accelerate convergence have introduced preconditioning filters based on singular value decomposition (SVD), aiming to decorrelate reference signals and decouple plant responses. While effective in some cases, these SVD-based filters are typically non-causal and require introducing additional delay. Thus, they are unsuitable for real-time ANC systems, where latency must be minimized. This work proposes a causal multichannel preconditioning filter design approach using spectral factorization of the reference signal cross-spectral matrix and a minimum-phase/all-pass decomposition of the secondary path. The approach leverages a numerically robust algorithm based on discrete-time Riccati equations to ensure causality without requiring additional delays. Simulation results demonstrate that the proposed filters substantially improve both the convergence speed and noise reduction performance of the LMS algorithm in real-time ANC applications.

Keywords: Active noise control (ANC), MIMO, Filtered-x least mean square (FxLMS) algorithm, Polynomial matrix spectral factorization,

*Corresponding author: yangfan@purdue.edu

[1]This work was done before the author joined Amazon and does not relate to the author's position at Amazon.

minimum phase filter, all-pass filter.

1. Introduction

Active noise control (ANC) technology has seen substantial progress in recent decades. It has been deployed successfully in a variety of commercial applications, including vehicle cabins [1, 2], consumer headphones [3, 4, 5], headrest-integrated systems [6, 7], and open windows [8, 9].

The least-mean-square (LMS) algorithm is among the most widely adopted adaptive filtering techniques. Besides active noise control (ANC) [10, 11], the LMS algorithm has found applications in various fields such as speech analysis [12, 13], cross-talk cancellation [14, 15], and adaptive equalization [16, 17] owing to its simplicity and effectiveness. Despite these advantages, one of the main drawbacks of the LMS algorithm in multiple-input-multiple-output (MIMO) systems is its slow convergence, particularly when broadband signals are involved [18, 19]. The filter adaptation speed is a key consideration for real-life applications with time-varying environments or systems [19], such as variable-speed HVAC equipment [20]. Prior research has extensively explored the convergence behavior of MIMO LMS algorithms [11, 21], and most studies agree that the sluggish convergence in ANC systems is mainly caused by two factors: the correlation between reference signals and the coupling between input-output channel pairs in the secondary path, which refers to the response from control sources to error microphones.

To address this challenge, Douglas et al. proposed a self-whitening algorithm that adaptively filters the reference signals prior to feeding them into the LMS algorithm [22]. Building on this concept, Bai and Elliott introduced a preconditioning approach that leverages singular value decomposition (SVD) to decorrelate the reference signals and decouple the secondary path responses [23]. While this SVD-based method effectively enhances convergence, it produces non-causal preconditioning filters. To ensure causality, artificial delays must be manually incorporated, which restricts its practicality to applications where system delays have minimal impact, such as spatial audio. However, in real-time ANC systems, where noise attenuation performance is highly sensitive to delay [24], this limitation becomes a significant obstacle.

An alternative strategy to avoid introducing extra delay is to employ spectral factorization on the estimated cross-spectral density matrix of the

reference signals, which yields a minimum-phase matrix. The inverse of this matrix can serve as a causal prewhitening filter. Similarly, the frequency response matrix of the secondary path can be decomposed into minimum-phase and all-pass components, which can be used to eliminate inter-channel coupling. The key advantage of this method is that it generates causal preconditioning filters with minimal delay without the need for delay adjustments. However, for general MIMO systems with broadband signals, no numerically stable algorithms had been available for performing this decomposition, limiting prior applications to relatively simple systems where the minimum-phase/all-pass decomposition could be derived analytically or by observation [21]. As a result, this approach has not yet been applied in real-time ANC scenarios involving practical broadband reference signals and complex secondary path models.

One major challenge in applying minimum-phase decomposition to MIMO preconditioning lies in the mathematical complexity: both the cross-spectral matrix of the reference signals and the secondary path frequency response matrix must first be approximated by high-order polynomials or rational functions in the z-domain. Performing accurate minimum-phase decomposition on these high-order matrices is computationally intensive and numerically sensitive. The problem of spectral factorization has been studied extensively by both signal processing and mathematical communities. For single-input-single-output (SISO) systems, zeros outside the unit circle are simply reflected inward during decomposition. However, this method becomes unreliable for high-order polynomials, where numerical errors can prevent accurate root calculation [25, 26, 27]. Following Wiener's foundational introduction of spectral factorization [28], alternative algorithms have been developed that do not require root solving, as summarized in [29], offering more robust solutions for high-order SISO systems. Additionally, the minimum-phase component of the power spectral density can be computed directly in the cepstrum domain, bypassing explicit polynomial modeling altogether [11].

For MIMO systems, Wiener later extended the spectral factorization concept to multivariate cases [30], though the mathematical complexity increases substantially compared to SISO systems. One of the earliest constructive solutions for MIMO spectral factorization was proposed by Youla, who utilized the Smith canonical form of polynomial matrices [31]. Nevertheless, Youla's method proves to be computationally intensive and difficult to apply when matrix orders are large. Building on Wiener's and Youla's contributions, various algorithms for MIMO spectral factorization have since been devel-

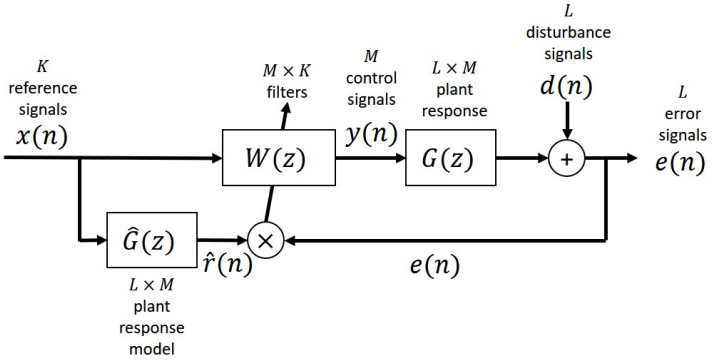

Figure 1: Filtered-reference LMS algorithm.

oped and summarized in [32]. More recently, efforts have been made to reduce the computational cost of these factorizations [33, 34, 35]. Among these advancements, the family of methods based on solving Riccati equations, as summarized by Kailath [36], offers particular advantages thanks to its structured formulation and the availability of efficient algorithms for solving discrete-time algebraic Riccati equations (DARE) [37]. This state-space-based approach also enables a smooth extension from SISO to MIMO systems, leveraging the theoretical framework established by Kalman [38].

In this study, a new method is presented for designing causal preconditioning filters for both the reference signals and the secondary path in a real-time MIMO ANC system. This approach is based on performing spectral factorization by solving discrete-time Riccati equations, followed by time-domain conversion of the resulting filters. These filters are then incorporated into the filtered-reference LMS (FxLMS) algorithm to enhance its convergence rate during adaptive learning. Both simulation and experiment were implemented to demonstrate the effectiveness of the proposed method.

2. Theory

2.1. Review of Filtered-reference LMS algorithm

Figure 1 shows a standard FxLMS algorithm. The discrete-time reference signals collected by K sensors are

$$\mathbf{x}(n) = [x_1(n) \quad ... \quad x_K(n)]^T, \tag{1}$$

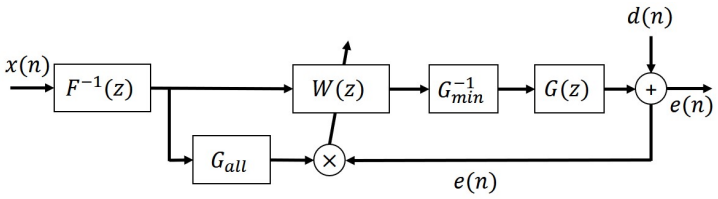

Figure 2: Active noise control system using preconditioned Filtered-reference LMS algorithm.

where n is the time index. The $\mathbf{x}(n)$ is filtered by a K-input-M-output ANC filter to generate M control signals $\mathbf{y}(n)$:

$$\mathbf{y}(n) = [y_1(n) \quad ... \quad y_M(n)]^T. \tag{2}$$

The control signal $\mathbf{y}(n)$ is used as the input to the secondary path $\mathbf{G}(z)$. The secondary path response is described using an $L \times M$ matrix $\mathbf{G}(z)$ where L is the number of error microphones. $\mathbf{G}(z)$ includes the responses of speakers and microphones, analog and digital pre-processing effects, and the acoustic propagation effect.

When the ANC system is not activated, the L disturbance signals can be expressed by

$$\mathbf{d} = [d_1(n) \quad ... \quad d_L(n)]^T. \tag{3}$$

After the ANC system is activated, the error signal vector can be represented as

$$\mathbf{e} = [e_1(n) \quad ... \quad e_L(n)]^T, \tag{4}$$

whose power is to be minimized for the most optimal ANC filter design. The adaptation rule for one of the most common adaptive ANC algorithms, FxLMS, can be written as

$$w_{mk}(n+1) = w_{mk}(n) - \mu \sum_{l=1}^{L} [e_l(n) r_{lmk}(n)], \tag{5}$$

where w_{mk} is the impulse response of the ANC filter $\mathbf{W}(z)$. r_{lmk} is the discrete convolution result of the modeled plant impulse responses and the reference signals (thus, filtered-reference), which is expressed as

$$r_{lmk}(n) = \sum_{j=0}^{J-1} \hat{g}_{lmj}(n) x_k(n-j), \tag{6}$$

where $\hat{g}_{lmj}$ is the impulse response of the modeled secondary path, $\hat{\mathbf{G}}(z)$ with the m-th control signal, the l-th output channel at the j-th time sample.

The convergence rate of multichannel LMS algorithms suffers from the correlation of reference signals and the coupling of the plant responses. The problem can be resolved in [23] by adding two preconditioning filters into the LMS system, which can be obtained by applying singular value decomposition to the cross spectral density matrix of the reference signals $\mathbf{S}_{xx}(f)$ and the plant response matrix $\mathbf{G}(f)$. However, carefully chosen delays must be applied to the two preconditioning filters since the filters derived from the singular value decomposition are not necessarily causal, which can be an issue in real-time ANC applications and other delay-sensitive applications.

2.2. Causal multichannel preconditioning filters for FxLMS algorithms

To apply the preconditioning filtering method in real-world ANC systems and improve the convergence rate of the FxLMS algorithm, it is essential to design causal preconditioning filters with minimal delay. A schematic of an FxLMS system incorporating such causal preconditioning filters is shown in Fig. 2. In this approach, the matrix $\mathbf{F}(z)$, derived from the cross-spectral density matrix of the reference signals $\mathbf{S}_{xx}(z)$, is designed as a minimum-phase system. The process of obtaining $\mathbf{F}(z)$ from $\mathbf{S}_{xx}(z)$ is known as spectral factorization and is expressed as

$$\mathbf{S}_{xx}(z) = \mathbf{F}(z)\mathbf{F}^{\mathrm{T}}(1/z), \tag{7}$$

where,

$$\mathbf{S}_{xx}(z) = E[\mathbf{x}(z)\mathbf{x}^{\mathrm{T}}(1/z)], \tag{8}$$

$\mathbf{x}(z)$ is the z transformed references signals $\mathbf{x}(n)$, and E is the expectation operator. Through spectral factorization, the reference signals $\mathbf{x}(n)$ can be viewed as the output of uncorrelated white noise signals $\mathbf{v}(n)$, each with unit power, passed through a minimum-phase shaping filter $\mathbf{F}(z)$ [11], i.e.,

$$\mathbf{x}(z) = \mathbf{F}(z)\mathbf{v}(z). \tag{9}$$

It is worth noting that the cross-spectral density matrix of the white noise signals $\mathbf{v}(n)$ is $\mathbf{S}_{vv}(z) = \mathbf{I}_K$, where $\mathbf{I}_K$ denotes the $K \times K$ identity matrix.

Since $\mathbf{F}(z)$ is both causal and minimum-phase, its inverse $\mathbf{F}^{-1}(z)$ also shares these properties. The reference signals can therefore be whitened using $\mathbf{F}^{-1}(z)$ as

$$\mathbf{v}(z) = \mathbf{F}^{-1}(z)\mathbf{x}(z), \tag{10}$$

where $\mathbf{F}^{-1}(z)$ represents the inverse system of $\mathbf{F}(z)$. The whitened reference signals $\mathbf{v}(z)$ can then serve as the new inputs for the FxLMS algorithm. Since these signals are uncorrelated, the convergence rate is significantly improved. This improvement is primarily attributed to the reduced eigenvalue spread of the reference signal's auto-correlation matrix [11].

For the secondary path responses $\mathbf{G}(\mathbf{z})$, it can be decomposed into an $M \times M$ minimum phase filter matrix $\mathbf{G}_{min}(z)$ and the $L \times M$ all-pass filter matrix $\mathbf{G}_{all}(z)$:

$$\mathbf{G}(z) = \mathbf{G}_{all}(z)\mathbf{G}_{min}(z). \tag{11}$$

Note that the all-pass filter matrix satisfies the condition $\mathbf{G}_{\text{all}}^{T}(z)\mathbf{G}_{\text{all}}(z) = \mathbf{I}_{M}$. In the proposed FxLMS algorithm (referred to hereafter as "the proposed LMS"), the filter coefficients are updated using the same form as Eq. 5. The only difference is that, instead of the original reference signals filtered by $\mathbf{G}(z)$, the algorithm uses a new set of filtered reference signals, computed as

$$r_{lmk}(n) = \sum_{j=0}^{J-1} g_{all,lmj} v_k(n-j), \tag{12}$$

where $g_{all,lmj}$ is the lmj-th entry of the all-pass component in the time domain, and v_k is the k-th signal of the whitened reference signal. Similar to Eq. 7, the all-pass component and the minimum phase component of the $\mathbf{G}(z)$ matrix can be obtained by performing spectral factorization to matrix $\mathbf{G}^{\text{H}}(z)\mathbf{G}(z)$. The details of the decomposition process will be discussed in Sec. 2.3.

The above mentioned preconditioning process depends on a convenient and numerically stable algorithm to perform the spectral factorization of $\mathbf{S}_{xx}(z)$ and the minimum phase/all-pass decomposition of $\mathbf{G}(z)$. A simple decomposition example was given by Elliot [21] for two pink noise reference signals and simple secondary path response functions obtained from a free field sound propagation model, where the spectral factorization and the minimum phase/all-pass decomposition can be accomplished via observation. For more complicated reference signals and secondary path responses, which are very common for broadband multi-channel ANC applications, these two types of decomposition cannot be performed easily. However, with the decomposition algorithm in state-space representation and advances in recent years in solving discrete Riccati equations, the preconditioning filter design becomes practically feasible for complicated broadband sound sources and plant responses.

2.3. Realization of spectral factorization and minimum phase/ all-pass decomposition

The numerical algorithm used in the proposed work to perform the spectral factorization and the minimum phase/ all-pass decomposition requires both the cross spectral density matrix, $\mathbf{S}_{xx}(z)$, and the plant response matrix, $\mathbf{G}(z)$ to be in a polynomial form. The polynomial representations of these two matrices can be obtained through a system identification process described in Section 2.4. In this subsection, numerical methods to perform each decomposition is introduced under the assumption that polynomial representations of $\mathbf{S}_{xx}(z)$ and $\mathbf{G}(z)$ are already found.

The cross spectral density matrix $\mathbf{S}_{xx}(z)$ can be expressed as a polynomial matrix of order q as

$$\mathbf{S}_{xx}(z) = \sum_{i=-q}^{q} \mathbf{R}_i z^{-i}, \tag{13}$$

where $\mathbf{R}_i$ is a constant matrix with the same dimension as $\mathbf{S}_{xx}(z)$. If the polynomial matrix $\mathbf{S}_{xx}(z)$ satisfies the following conditions:

1. $\mathbf{S}_{xx}(z) = \mathbf{S}_{xx}^T(1/z)$; (The property is sometimes named as paraconjugate or Hermitian symmetric by different authors)
2. $\mathbf{S}_{xx}(z)$ must be analytic and positive definite on the unit circle;

then a canonical spectral factorization $\mathbf{F}(z)$ must exist. Besides, the matrix $\mathbf{F}(z)$ can be proved to be unique up to a constant right unitary multiplier [33, 34]. These two conditions are satisfied by broadband reference signals in practical ANC applications, so it is assumed in the study that a spectral factorization decomposition of reference $\mathbf{S}_{xx}(z)$ always exists.

It is worth mentioning that for a single-input-single-output system, the spectral factorisation can be calculated in the discrete frequency domain by using a cepstral method involving a discrete Hilbert transform [39, 11]. The expression for discrete version of $\mathbf{F}(z)$ is

$$\mathbf{F}(k_f) = \exp\{\mathrm{FFT}[c(n)\mathrm{IFFT} \cdot \ln(\mathbf{S}_{xx}(k_f))]\}, \tag{14}$$

where FFT and IFFT are the discrete Fourier transform and inverse discrete Fourier transform, respectively. The causality constraint is given by $c(n) = 0$ for $n < 0$, $c(n) = 1$ for $n > 0$ and $c(0) = \frac{1}{2}$, and k_f is the discrete frequency index. An obvious disadvantage of the method is that it is only applicable to a single-channel reference signal.

Several algorithms have been derived for multi-channel $\mathbf{S}_{xx}(z)$ both in the continuous s domain and discrete z domain [31, 40, 33, 36, 34]. A method relying on solving for the stable solution of the discrete algebraic Riccati equation [36] is chosen for this study after comparing the speed, accuracy, and convenience in implementation for different spectral factorization approaches.

The steps of the numerical method for spectral factor decomposition used in the current work are briefly outlined here, more detailed explanations of this method can be found in [32]. The method is based on the theoretical result that, for a polynomial matrix $\mathbf{S}_{xx}(z)$ as described in Eq. 13, the decomposition expressed in Eq. 7 can be written into an equivalent expression as

$$\mathbf{S}_{xx}(z) = \mathbf{L}(z)\mathbf{R}_e\mathbf{L}^T(1/z), \tag{15}$$

where $\mathbf{R}_e$ is a symmetric constant positive definite matrix and $\mathbf{L}(z)$ is a minimum phase system defined with an expression

$$\mathbf{L}(z) = \mathbf{I}_K + \mathbf{L}_1 z^{-1} + ... + \mathbf{L}_q z^{-q} = \mathbf{I}_K + \sum_{i=1}^{q} \mathbf{L}_i z^{-i}. \tag{16}$$

It should be noted that although $\mathbf{S}_{xx}(z)$ is expressed as a polynomial matrix here, spectral factorization also exist for non-polynomial functions if it satisfies a finite-power and Paley-Wiener condition [29]. However, only the polynomial form of $\mathbf{S}_{xx}(z)$ is considered in this study.

Obtaining the minimum phase spectral factor matrix $\mathbf{F}(z)$ is now equivalent to solving for the coefficients matrices $\mathbf{L}_i$ and the constant matrix $\mathbf{R}_e$ in Eq. 15 and Eq. 16. The two sets of coefficient matrices can be calculated with a three-step procedure:

1. Define the following matrices $\mathbf{C}, \mathbf{h}, \bar{\mathbf{N}}$.
   The expression of $\mathbf{C}$ is

$$\mathbf{C} = \begin{bmatrix} \mathbf{0}_K & & & \\ \mathbf{I}_K & \mathbf{0}_K & & \\ & ... & ... & \\ & & \mathbf{I}_K & \mathbf{0}_K \end{bmatrix}, \tag{17}$$

   where $\mathbf{0}_K$ is a zero valued matrix of size $K \times K$ and the dimension of $\mathbf{C}$ is $Kq \times Kq$. It should be noted that each entry of matrix $\mathbf{C}$ is a block of size $K \times K$ instead of a scalar for multichannel reference signals.

The expression of $\mathbf{h}$ is simply

$$\mathbf{h} = \begin{bmatrix} \mathbf{0}_K & \mathbf{0}_K & ... & \mathbf{0}_K & \mathbf{I}_K \end{bmatrix}, \tag{18}$$

where the total length of $\mathbf{h}$ is $K \times q$.
The $\bar{\mathbf{N}}$ matrix is defined as

$$\bar{\mathbf{N}} = \begin{bmatrix} \mathbf{R}_q \\ \mathbf{R}_{q-1} \\ ... \\ \mathbf{R}_1 \end{bmatrix}, \tag{19}$$

where each entry is also a $K \times K$ matrix and is defined in Eq. 13.

2. Solve the stabilizing solution $\mathbf{\Sigma}$ of the discrete algebraic Riccati equation:

$$\mathbf{\Sigma} = \mathbf{C}\mathbf{\Sigma}\mathbf{C}^{\mathrm{H}} - (\mathbf{C}\mathbf{\Sigma}\mathbf{h}^{\mathrm{H}} - \bar{\mathbf{N}})(\mathbf{h}\mathbf{\Sigma}\mathbf{h}^{\mathrm{H}} - \mathbf{R}_0)^{-1}(\mathbf{C}\mathbf{\Sigma}\mathbf{h}^{\mathrm{H}} - \bar{\mathbf{N}})^{\mathrm{H}} \tag{20}$$

such that the matrix

$$\mathbf{C}_p = \mathbf{C} - (\mathbf{C}\mathbf{\Sigma}\mathbf{h}^{\mathrm{H}} - \bar{\mathbf{N}})(\mathbf{h}\mathbf{\Sigma}\mathbf{h}^{\mathrm{H}} - \mathbf{R}_0)^{-1}\mathbf{h} \tag{21}$$

has all its eigenvalues strictly inside the unit circle. The H superscription is the Hermitian operator. In this study, Eq. 20 is solved with the method of invariant subspace [41].

3. Then the required constant matrix $\mathbf{R}_e$ and the coefficients matrices $\mathbf{L}_i$ in Eq. 15 can be obtained as:

$$\mathbf{R}_e = \mathbf{R}_0 - \mathbf{h}\mathbf{\Sigma}\mathbf{h}^{\mathrm{H}}, \quad \mathbf{g} = (\bar{\mathbf{N}} - \mathbf{C}\mathbf{\Sigma}\mathbf{h}^{\mathrm{H}})\mathbf{R}_e^{-1}, \tag{22}$$

where $\mathbf{g}$ contains the coefficient matrices $\mathbf{L}_i$ with $i = 1$ to q, and its expression is

$$\mathbf{g} = \begin{bmatrix} \mathbf{L}_q \\ \mathbf{L}_{q-1} \\ ... \\ \mathbf{L}_1 \end{bmatrix}. \tag{23}$$

In a similar way, the minimum-phase and all-pass decomposition of the plant response matrix $\mathbf{G}$ can be obtained by applying spectral factorization to the para-conjugate matrix:

$$\mathbf{G}^{\mathrm{H}}(z)\mathbf{G}(z) = \mathbf{G}_{min}^{\mathrm{H}}(z)\mathbf{G}_{min}(z). \tag{24}$$

The spectral factorization of $\mathbf{G}^{\mathrm{H}}(z)\mathbf{G}(z)$ yields the minimum-phase component of the plant response matrix, $\mathbf{G}_{\min}(z)$. The all-pass component can then be determined as

$$\mathbf{G}_{all} = \mathbf{G}(z)\mathbf{G}_{min}^{-1}(z). \tag{25}$$

The expression of the $\mathbf{G}_{all}$ matrix satisfies the property of all-pass filter:

$$\mathbf{G}_{all}(z)^{\mathrm{H}}\mathbf{G}_{all}(z) = \mathbf{I}_L, \tag{26}$$

where $\mathbf{I}_L$ is an identity matrix with a dimension of $L \times L$.

2.4. System identification of $\mathbf{S}_{xx}(z)$ *and* $\mathbf{G}(z)$

The prerequisite condition for the decomposition processes described in Sec. 2.3 is an accurate modeling of $\mathbf{S}_{xx}(z)$ and $\mathbf{G}(z)^{\mathrm{H}}\mathbf{G}(z)$ in polynomial matrix form as described in Eq. 13. The modeling of $\mathbf{S}_{xx}(z)$ is different from the system identification of the plant transfer matrix, since $\mathbf{S}_{xx}(z)$ needs to be paraconjugate and positive definite on the unit circle. To satisfy the paraconjugate condition, a Cholesky decomposition can be applied to the frequency domain $\mathbf{S}_{xx}(e^{j\omega})$, which can be obtained from signal measurements. The Cholesky decomposition can be expressed as

$$\mathbf{S}_{xx}(e^{j\omega}) = \mathbf{S}(e^{j\omega})\mathbf{S}^{\mathrm{H}}(e^{j\omega}). \tag{27}$$

Then a time delay term is multiplied to the Cholesky decomposed matrix to ensure that each entry of the $\mathbf{S}(e^{j\omega})e^{j\omega\Delta}$ matrix is causal and can be modeled by an FIR filter with least square method or other approaches. It should be noted that adding the delay Δ is merely a modeling trick to construct a polynomial matrix $\mathbf{S}_{xx}(z)$. This does not affect the causality of the derived $\mathbf{F}(z)$ in subsequent steps and does not introduce any additional delay to the ANC filter in real-time implementation. After approximating $\mathbf{S}(e^{j\omega})e^{j\omega\Delta}$ by a polynomial matrix $\mathbf{B}(z)$, the cross spectral density matrix in z domain, $\mathbf{S}_{xx}(z)$, can then be calculated by

$$\mathbf{S}_{xx}(z) = \mathbf{B}(z)\mathbf{B}^{\mathrm{T}}(1/z). \tag{28}$$

It is noted that the time delay term $e^{j\omega\Delta}$ is canceled out in this process. The $\mathbf{G}(z)^{\mathrm{H}}\mathbf{G}(x)$ matrix can be modeled by the same approach. Then the expression of $\mathbf{G}_{min}$ and $\mathbf{G}_{all}$ can be derived by the same spectral factorization algorithm.

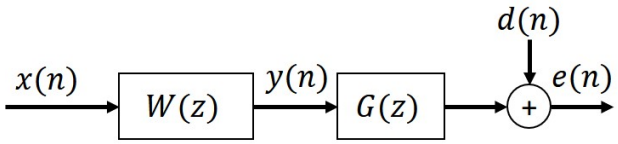

Figure 3: Feedforward control system.

2.5. Optimal solution in the frequency domain

Since the spectral factorization technique is already available, the optimum solution in the frequency domain for a stationary system can also be obtained. The optimum solution for the causal Wiener filter for an active noise control system can be expressed as [11]

$$\mathbf{W}_{opt}(z) = -\mathbf{G}_{min}^{-\mathrm{H}}\{\mathbf{G}_{all}^{\mathrm{H}}\mathbf{S}_{xd}(z)\mathbf{F}^{-1}(z)\}_{+}\mathbf{F}^{-1}(z). \tag{29}$$

where the $_+$ subscript suggests that only the causal component of the function in the bracket should be kept.

Indeed, Eq. 29 can be used to obtain the optimum controller coefficient in a stationary feedforward system described in Fig. 3. However, the optimum solution is found to be much more sensitive to the modeling errors of $\mathbf{S}_{xx}(z)$, $\mathbf{S}_{xd}(z)$ and $\mathbf{G}(z)$ compared with the solution obtained by the proposed preconditioning FxLMS algorithm because the adaptive algorithm can compensate the modeling error in real time.

3. Results

This section presents two parts. The first part uses simple white noise and pink noise source models along with free-field propagation models for the secondary path. In this case, the all-pass and minimum-phase decomposition of the plant response can be verified through direct observation. The primary goal of this simulation is to validate the proposed spectral factorization approach against analytical solutions for both the all-pass and minimum-phase components. In the second part, an experimentally measured realistic plant response is used to demonstrate that the decomposition method is applicable to practical and more complex secondary path models.

The code used to obtain the causal and low-delay $\mathbf{G}_{min}$, $\mathbf{G}_{all}$, and $\mathbf{F}^{-1}$ are available on GitHub[2].

[2] `https://github.com/Yongjie-Zhuang/Causal-preconditioning-FxLMS`

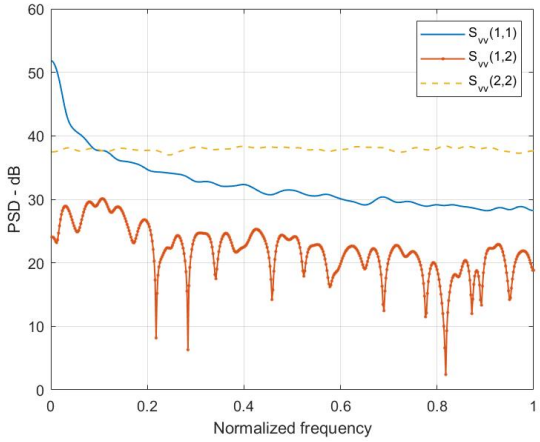

Figure 4: Different elements in the cross spectral density matrix, $\mathbf{S}_{vv}(z)$, of a pink noise and a white noise sources.

3.1. Simulation study on systems with a simple plant response

A numerical simulation is carried out to validate the key steps of the proposed preconditioning filter design for multichannel LMS algorithms (illustrated in Fig. 2) and to demonstrate the resulting improvement in convergence rate. The sampling rate of the simulation, f_s, is chosen to be 1 kHz. Two independent input signals are used: a white noise sequence and an uncorrelated pink noise sequence, represented as $\mathbf{v}(n) = [v_1(n), v_2(n)]^{\mathrm{T}}$. Different elements in the cross spectral density matrix of the two source signals are shown in Fig. 4. It can be observed that the two signals are uncorrelated because the off-diagonal term $\mathbf{S}_{vv}(1,2)$ is much smaller than diagonal terms $\mathbf{S}_{vv}(1,1)$ and $\mathbf{S}_{vv}(2,2)$. The two sources are then combined using a mixing filter M, defined as

$$M = \begin{bmatrix} 0.75 & 0.3 \\ 0.3 & 1 \end{bmatrix}. \tag{30}$$

The resulting mixed signals, $x_1(n)$ and $x_2(n)$, are then used as reference inputs for the preconditioning LMS system.

As illustrated in Fig. 5, two error microphones are symmetrically arranged. The secondary path adopts the same transfer functions as those used by Bai and Elliott [23], given by

$$\mathbf{G}(z) = \begin{bmatrix} z^{-N_1} & \frac{l_1}{l_2} z^{-N_2} \\ \frac{l_1}{l_2} z^{-N_2} & z^{-N_1} \end{bmatrix}. \tag{31}$$

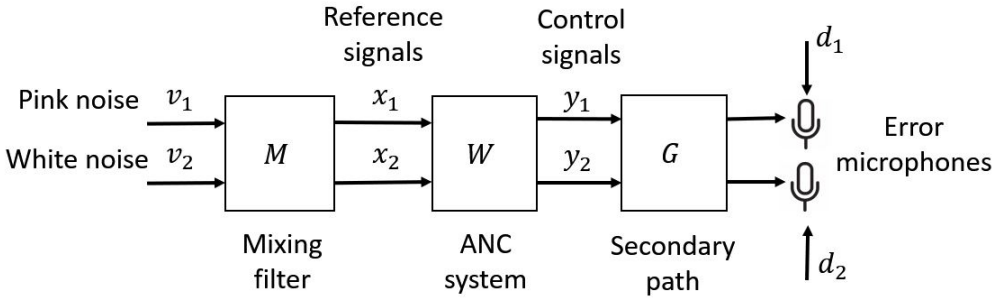

Figure 5: Simulation arrangement for the preconditioning Filtered-reference LMS algorithm.

Here, N_1 and N_2 are the nearest integer values of $l_1 f_s/c_0$ and $l_2 f_s/c_0$, respectively, where $l_1 = 2, \mathrm{m}$ and $l_2 = 3, \mathrm{m}$ represent the distances from the first secondary source to the first and second error microphones. The speed of sound in the air is assumed to be $c_0 = 340, \mathrm{m/s}$. Due to the symmetric arrangement of the secondary sources and error microphones, the matrix $\mathbf{G}(z)$ is also symmetric. The disturbance signals $d_1(n)$ and $d_2(n)$ are computed using the same transfer functions as in Eq. 31, but with $l_1 = 3, \mathrm{m}$ and $l_2 = 4, \mathrm{m}$.

After applying the mixing matrix, the reference signal becomes correlated. The magnitude of each term in the S_{xx} matrix are shown in Fig. 6. It can be observed that the coupling term $\mathbf{S}_{xx}(1,2)$ is larger than $\mathbf{S}_{xx}(1,1)$ over a wide frequency range, which suggests the two channels are highly correlated.

The $\mathbf{S}_{xx}$ matrix in polynomial form is identified using the techniques outlined in Sec. 2.4. The resulting $\mathbf{S}xx(z)$ is then decomposed via spectral factorization by solving the associated discrete Riccati equation, as described in Sec. 2.3. The resulting decomposition matrix $\mathbf{F}(z)$ is minimum-phase, allowing its inverse $\mathbf{F}^{-1}(z)$ to serve as a causal prewhitening filter for the reference signals.

The frequency response magnitude and the phase of each entry in $\mathbf{F}^{-1}$ is plotted in Fig. 7. The $(1,1)$ term has an obvious high pass characteristic which is to whiten the pink noise source signal. Also, the whitening filters are different for different channels. The causality of these prewhitening filters can be seen in the impulse response plot of $\mathbf{F}^{-1}$ shown in Fig. 8. In this simulation, the length of the prewhitening filters is chosen to be a constant, 100. It can be observed that the filter response is zero at the end of the

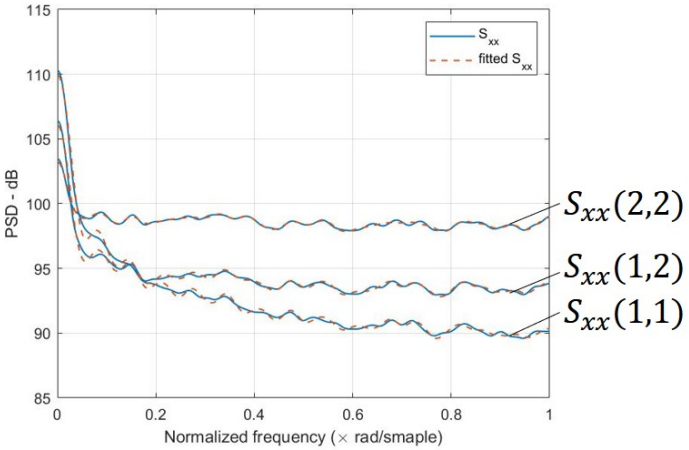

Figure 6: Power spectral density $\mathbf{S}_{xx}(z)$ of reference signals. Solid lines: calculated PSD; Dashed lines: fitted PSD function.

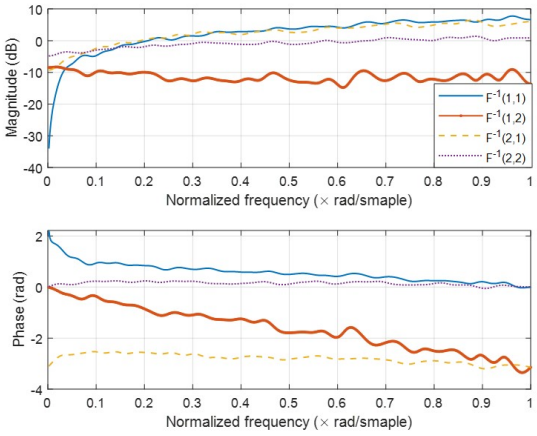

Figure 7: Frequency response of the prewhitening filter $\mathbf{F}^{-1}$

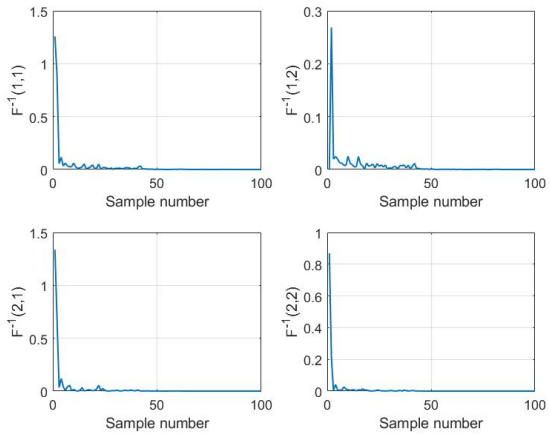

Figure 8: Impulse response of the prewhitening filter $\mathbf{F}^{-1}$

filter sequence, and all the impulse functions decays to zero quite rapidly. Since no delay is required to satisfy the causality condition of the filter, the prewhitening filter can be directly implemented in real time if the cross spectral density matrix $\mathbf{S}_{xx}(z)$ of the reference signals is known or measured. This is a key advantage compared with other prewhitening techniques, such as the singular value decomposition based prewhitening filter [23], which requires adding plentiful delays to make the filters causal for implementation.

The reference signals are then passed through the prewhitening filter $\mathbf{F}^{-1}(z)$, producing a new pair of signals, $\bar{v}_1$ and $\bar{v}_2$, whose power spectral densities are shown in Fig. 9. As observed, the power levels of $\mathbf{S}_{\bar{v}\bar{v}}(1,1)$ and $\mathbf{S}_{\bar{v}\bar{v}}(2,2)$ are nearly constant, indicating successful whitening. Additionally, the off-diagonal term $\mathbf{S}_{\bar{v}\bar{v}}(1,2)$ is over 10 dB lower than the diagonal elements, further confirming that the signals are effectively decorrelated.

The next step is to eliminate the coupling in the secondary path through a minimum-phase/all-pass decomposition. According to the procedures detailed in Sec. 2.3, the minimum-phase component $\mathbf{G}_{min}$ is first derived using the spectral factorization method. The corresponding all-pass component $\mathbf{G}_{all}(z)$ is then obtained from Eq. 25. In the simulation, the impulse response of the plant response function $\mathbf{G}(z)$ is shown in Fig. 10, and the impulse response of $\mathbf{G}_{all}(z)$, modeled as a FIR filter, is illustrated in Fig. 11. It can be seen that the impulse response values of $\mathbf{G}_{all}(1,1)$ and $\mathbf{G}_{all}(2,2)$ are nearly zero except at the N_1th sample, consistent with the analytical result

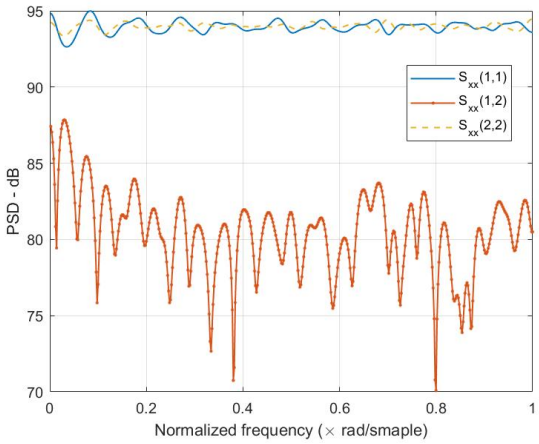

Figure 9: Power spectral density $\mathbf{S}_{\bar{v}\bar{v}}(z)$ of the filtered reference signals.

derived from observation [21]:

$$\mathbf{G}_{all} = \begin{bmatrix} z^{-N_1} & 0 \\ 0 & z^{-N_1} \end{bmatrix}. \tag{32}$$

Similar to the prewhitening filter $\mathbf{F}^{-1}(z)$, according to Eq. 25, $\mathbf{G}_{all}(z)$ filter can be obtained from $\mathbf{G}(z)$ without requiring additional time delays to be applied to the filter to satisfy the causality condition, which means it can be used in real-time ANC applications if the secondary path is properly modeled offline or online.

To illustrate the enhancements in ANC performance and convergence speed achieved by the proposed preconditioning filters, the sound pressure level at the first error microphone is displayed in Fig. 12. The curves a through e represent the sound pressure levels (SPLs) of the disturbance signal, the error signal from the conventional LMS algorithm, the error signal from the LMS algorithm with $\mathbf{G}_{min}^{-1}$ and $\mathbf{G}_{all}$ applied, the error signal with $\mathbf{F}^{-1}$ applied, and the error signal using all three filters: $\mathbf{G}_{min}^{-1}$, $\mathbf{G}_{all}$, and $\mathbf{F}^{-1}$, respectively. Each curve is averaged over 30 samples for improved clarity. The response observed at the second microphone is comparable and therefore omitted. The convergence coefficient (learning rate) μ should be manually selected. A higher convergence coefficient results in a faster convergence rate. However, a learning rate larger than the stability bound will lead to divergence of LMS algorithm. The convergence coefficient μ in Eq. 5

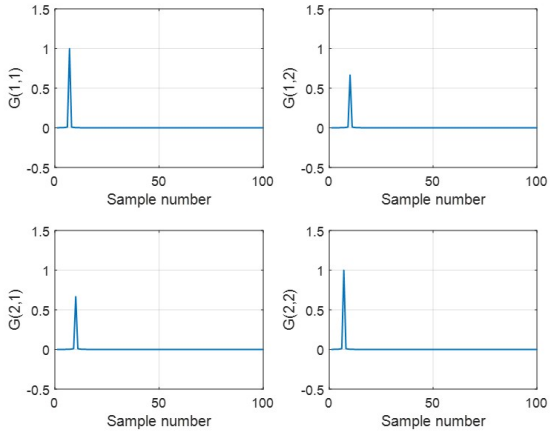

Figure 10: Impulse response of the plant response $\mathbf{G}(z)$.

is chosen as one-third of the minimum value that leads to instability to provide certain robustness. As shown in Fig. 12, the baseline LMS algorithm yields the lowest performance, achieving only about 10 dB of noise reduction after 4000 samples. With the addition of the prewhitening filter $\mathbf{F}^{-1}$, this improves to approximately 25 dB. Introducing $\mathbf{G}_{min}^{-1}$ and $\mathbf{G}_{all}$ alone results in a moderate improvement of around 14 dB, marginally outperforming the standard FxLMS algorithm. When both $\mathbf{F}^{-1}$, $\mathbf{G}_{min}^{-1}$, and $\mathbf{G}_{all}$ are applied, the reduction reaches 30 dB in just 2000 samples. In this scenario, the contribution of the prewhitening filter $\mathbf{F}^{-1}$ proves to be more impactful than that of the decoupling filters $\mathbf{G}_{all}$ and $\mathbf{G}_{min}^{-1}$.

3.2. Study on experimentally measured system response $\mathbf{G}(z)$

In the earlier simplified secondary path frequency response case, the secondary path is given based on the free-field propagation model. The results indicate that the spectral factorization method effectively performs the minimum-phase and all-pass decomposition for this type of frequency response. While an improvement can be observed with the inclusion of the secondary path decomposition, the enhancement is relatively modest, likely due to the limited coupling present in the secondary path.

In this section, an experimentally measured secondary path response is used to investigate the proposed method. In this case, a stronger inter-channel coupling of $\mathbf{G}(z)$ will allow a better illustration of the performance of the proposed method regarding the secondary path decoupling part. The

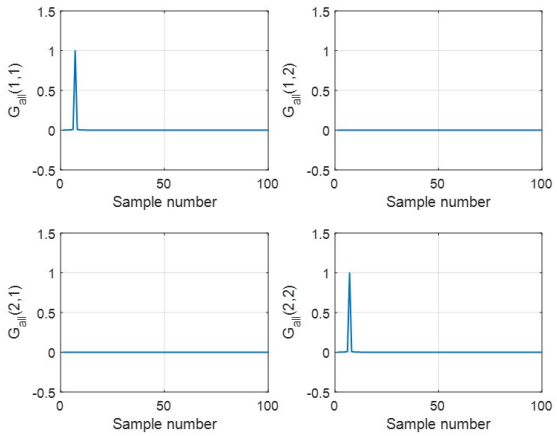

Figure 11: Impulse response of the all-pass component $\mathbf{G}_{all}(z)$.

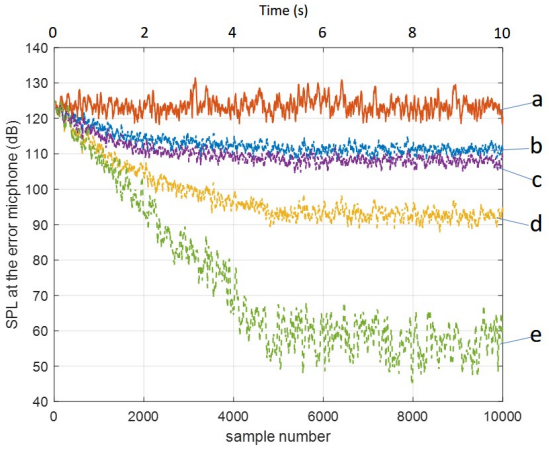

Figure 12: The SPLs measured at the microphone 1 in the first case of simplified secondary path responses. The four lines from top to bottom are: (a) when ANC system is not activated (original noise pressure level); (b) when conventional LMS algorithm is applied; (c) when LMS with $\mathbf{G}_{min}^{-1}$ and $\mathbf{G}_{all}$ is applied; (d) when LMS with $\mathbf{F}^{-1}$ is applied; (e) when LMS with $\mathbf{F}^{-1}$, $\mathbf{G}_{min}^{-1}$ and $\mathbf{G}_{all}$ is applied.

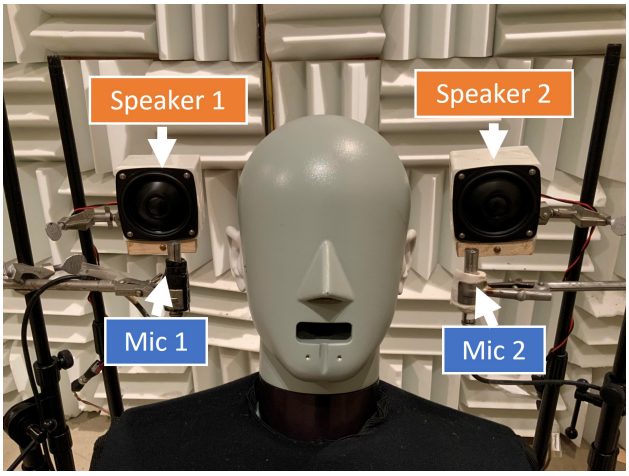

Figure 13: Experiment setup to measure the transfer function $\mathbf{G}(z)$.

experiment setup is shown in Fig. 13. Two loudspeakers are placed 15 cm away from the ears of the dummy. Two B&K 4189 microphones with TMS426B01 preamplifiers are placed 8 cm away from the ear horizontally. In the data acquisition stage, 25 kHz is used as the sampling frequency, and then the frequency up to 1500 Hz is used to model the frequency response function $\mathbf{G}(z)$. The measured plant response is fitted with 100 FIR coefficients as filter $\mathbf{G}(z)$. The impulse responses of the four components in $\mathbf{G}$ are plotted in Figure 14. It can be clearly observed that the magnitude in $\mathbf{G}(1,1)$ is less than that in $\mathbf{G}(1,2)$, which implies a strong coupling among different source-receiver pairs. Additionally, the reference signals and the disturbance signals used in this simulation are the same as those used in the first simulation.

The minimum-phase component $\mathbf{G}_{min}(z)$ and the all-pass component $\mathbf{G}_{all}(z)$ are extracted from the decomposition of $\mathbf{G}(z)$ using the spectral factorization approach outlined in Sec. 2.3. The corresponding impulse responses of $\mathbf{G}_{all}(z)$ and $\mathbf{G}_{min}^{-1}(z)$ are shown in Fig. 15 and Fig. 16, respectively. All decoupling filters are causal, and no additional delay compensation is required in their impulse responses.

A performance comparison across different FxLMS algorithm variants is presented in Fig.17. Similarly, the learning rate μ is set to half of the minimum value that leads to instability. The curves a through d represent the SPLs: (a) when ANC system is not activated (original noise pressure level); (b) when conventional LMS algorithm is applied; (c) when LMS with

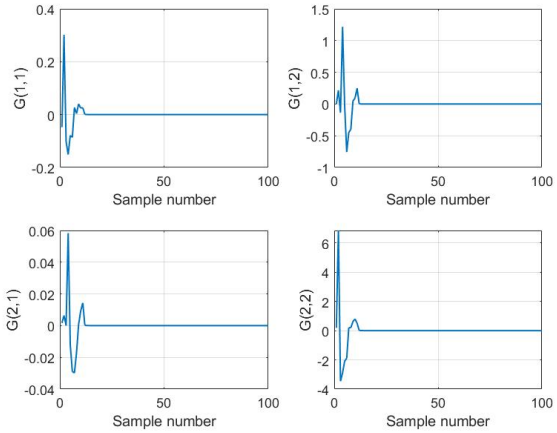

Figure 14: Impulse response of the secondary path $\mathbf{G}(z)$ (a 100-point FIR filter is used for each channel pair).

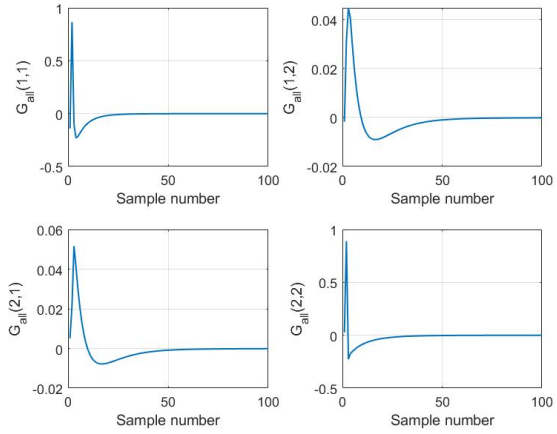

Figure 15: Impulse response of $\mathbf{G}_{all}(z)$ (a 100-point FIR filter is used for each channel pair).

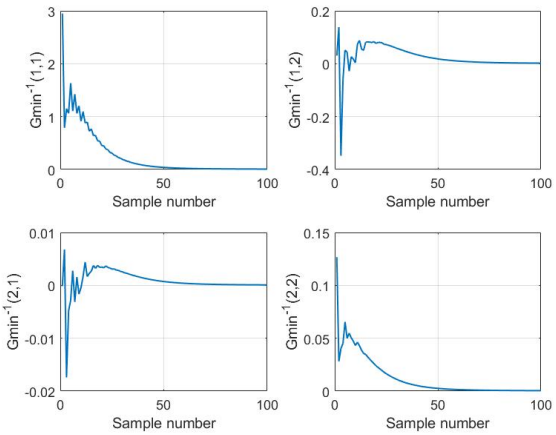

Figure 16: Impulse response of $\mathbf{G}_{min}^{-1}(z)$. A 100-point FIR filter is used for each channel.

$\mathbf{G}_{min}^{-1}$ and $\mathbf{G}_{all}$ is applied; (d) when LMS with $\mathbf{F}^{-1}$ is applied; when LMS with $\mathbf{F}^{-1}$, $\mathbf{G}_{min}^{-1}$ and $\mathbf{G}_{all}$ is applied, respectively. In this case, the conventional FxLMS algorithm fails to achieve effective noise reduction due to the strong coupling in both the reference signals and the realistic secondary path responses. When $\mathbf{G}_{min}^{-1}(z)$ and $\mathbf{G}_{all}(z)$ are incorporated, a reduction of approximately 10 dB is achieved after 4000 samples, indicating a notable improvement in convergence. In contrast, the use of the prewhitening filter $\mathbf{F}^{-1}(z)$ alone yields negligible improvement and is therefore excluded from the figure. When both reference and plant preconditioning filters are applied (curve d in Fig. 17), an additional 5 dB of noise reduction is observed relative to curve c, along with faster convergence. It is important to note, however, that the complexity of $\mathbf{G}(z)$ directly influences the length of the required preconditioning filters, highlighting a practical trade-off between computational cost and convergence performance in real-world implementations.

3.3. Potential for time varying signal and plant adaptation

Although the current work focuses on the techniques for off-line design of the preconditioning filters for active noise control, the potential of adaptively design these preconditioning filters to accommodate time varying signals and plants is briefly investigated here through the analysis of the computation time required by the preconditioning filter design process. It is clarified here that if the preconditioning filters are designed offline, the FxLMS algorithm

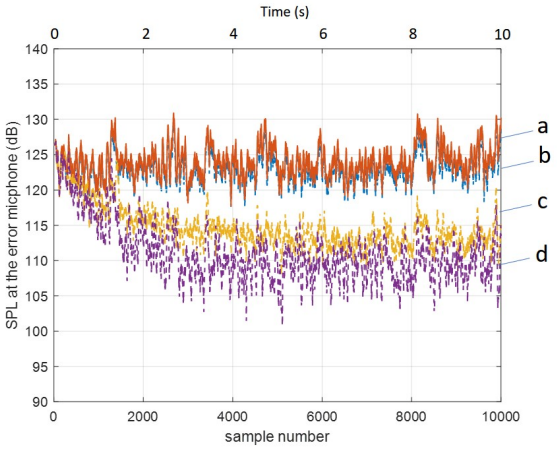

Figure 17: The SPLs measured at the microphone 1 in the second case of experimentally measured realistic secondary path responses. The four lines from top to bottom are: (a) when ANC system is not activated (original noise pressure level); (b) when conventional LMS algorithm is applied; (c) when LMS with $\mathbf{G}_{min}^{-1}$ and $\mathbf{G}_{all}$ is applied; (d) when LMS with $\mathbf{F}^{-1}$ is applied; (e) when LMS with $\mathbf{F}^{-1}$, $\mathbf{G}_{min}^{-1}$ and $\mathbf{G}_{all}$ is applied.

can still make the active noise control adaptive to the time varying characteristics of the primary path. However, adaptation potential discussed in this subsection refers to the ability to still maintain a good prewhitening performance if the reference signal is slowly varying in time and maintain a good decoupling performance if the secondary path is slowly varying.

In the two simulation cases described in this work, the LMS convergence can be reached after around 4s, and the time spent to calculate the spectral factorization of $\mathbf{S}_{xx}(z)$ and $\mathbf{G}^{\mathrm{H}}(z)\mathbf{G}(z)$ on a personal computer using Ryzen 3600x CPU is around 4 seconds. This means that, if sufficient computation power is available, the proposed preconditioning filter design method can also be implemented in the ANC applications adaptively by repeating the calculation based on updated reference signals and plant response models. For example, the preconditioning filters can be updated every 5 seconds when this personal computer using Ryzen 3600x CPU is used, and the decomposition can be calculated in parallel with the ANC FxLMS processing. From this result, it can be observed that the adaptation speed of repeatedly design the preconditioning filters is similar to the adaptation speed of the FxLMS algorithm. This is particularly suitable for stage-wise time-varying environments such as variable-speed HVAC equipment [20, 42].

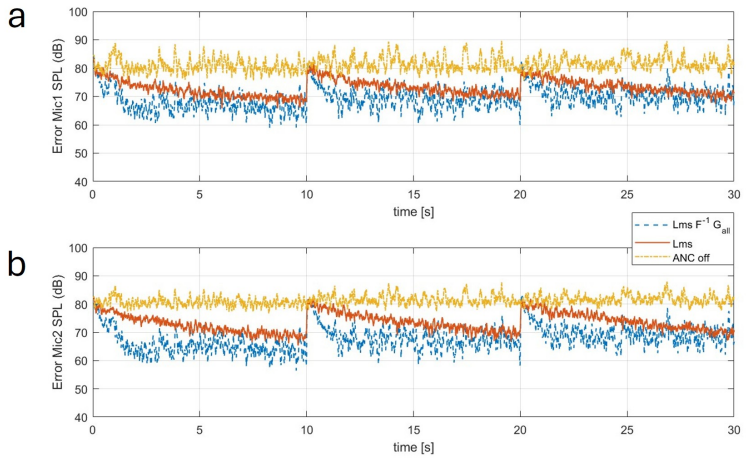

Figure 18: Sound pressure levels at the microphone 1 (a) and 2 (b) with primary path suddenly changed at 10 seconds and 20 seconds. The lines from top to bottom are when ANC system is not activated (original noise pressure level); when conventional LMS algorithm is applied; when LMS with $\mathbf{F}^{-1}$, $\mathbf{G}_{min}^{-1}$ and $\mathbf{G}_{all}$ is applied.

Finally, the robustness of the preconditioning algorithm is evaluated through a simulation in which the primary path of the system is altered every 10 seconds by moving the reference microphone one meter farther from the error microphones at each interval in Fig. 18. The preconditioning filters are not updated to demonstrate their robustness to the new primary path. Results show that the preconditioning filters still enhance the convergence speed of the LMS algorithm, despite being mismatched to the updated primary path. Notably, at 10 seconds, the preconditioned LMS outperforms the conventional LMS. However, by 30 seconds, its performance is comparable to that of the conventional LMS, indicating that the conventional LMS could exhibit slightly better robustness under substantial environmental changes.

4. Conclusion

This study proposes a prewhitening and preconditioning technique based on spectral factorization to enhance the convergence and performance of the filtered-reference LMS algorithm in real-time multichannel active noise control applications. The method involves decomposing the cross-spectral density matrix of the reference signals to obtain its minimum-phase spectral

factor by solving a discrete Riccati equation. The inverse of this spectral factor yields a causal, minimum-phase filter that serves as a prewhitening filter for the reference signals, enabling real-time implementation without additional delay compensation. A similar decomposition is applied to the secondary path to derive decoupling filters, which are also causal and delay-free. Results demonstrate that incorporating both the prewhitening and decoupling filters significantly accelerates convergence and improves noise reduction performance.

Compared to existing preconditioning methods such as [23], the proposed technique is better suited for real-life applications, as it avoids the need for manually added delays to ensure causality. Moreover, the approach is applicable to general cases involving complex reference signals and secondary path responses. Analysis of computational cost indicates that the decomposition can be performed within a time frame comparable to the convergence period of the LMS algorithm, allowing the filter design process to be repeated periodically. This makes the method suitable for slowly or stage-wise time-varying systems, where updated measurements of reference signals and plant models can be used to maintain effective preconditioning. In scenarios where the plant response remains stationary, the preconditioning filters may be computed offline in advance.

Future directions of this work include developing methods to adapt the preconditioning filters and LMS algorithm simultaneously in real-time. Additionally, integrating the proposed approach with frequency-domain FxLMS algorithms—particularly those employing delayless hybrid fast filtering and modified filtered-x structures—represents a promising direction for improving computational efficiency [43]. Finally, the stability constraints[44] associated with the proposed method under such extensions warrant further investigation.

References

[1] S. Zhang, L. Zhang, D. Meng, X. Zhang, A hybrid feedforward/feedback multi-channel active control system with optimization for cancelling road noise inside a vehicle cabin, Applied Acoustics 201 (2022) 109128.

[2] Q. Xu, S. Wang, J. Tao, H. Zou, X. Qiu, Creating personal sound zones in car cabins with active noise control, Applied Acoustics 235 (2025) 110670.

[3] X. Shen, D. Shi, S. Peksi, W.-S. Gan, A multi-channel wireless active noise control headphone with coherence-based weight determination algorithm, Journal of Signal Processing Systems 94 (8) (2022) 811–819.

[4] V. Patel, J. Cheer, A hybrid multi-reference subband control strategy for active noise control headphones, Applied Acoustics 197 (2022) 108932.

[5] Y. Zhuang, Y. Liu, A constrained optimal hear-through filter design approach for earphones, in: INTER-NOISE and NOISE-CON congress and conference proceedings, Vol. 263, Institute of Noise Control Engineering, 2021, pp. 1329–1337.

[6] Z. Zhang, M. Wu, L. Yin, C. Gong, J. Wang, S. Zhou, J. Yang, Robust feedback controller combined with the remote microphone method for broadband active noise control in headrest, Applied Acoustics 195 (2022) 108815.

[7] Y. Zhuang, X. Wang, Y. Liu, Singular vector filtering method for mitigation of disturbance enhancement in multichannel active noise control systems, Noise Control Engineering Journal 69 (5) (2021) 451–459.

[8] H. M. Lee, Y. Hua, Z. Wang, K. M. Lim, H. P. Lee, A review of the application of active noise control technologies on windows: Challenges and limitations, Applied Acoustics 174 (2021) 107753.

[9] D. Shi, B. Lam, K. Ooi, X. Shen, W.-S. Gan, Selective fixed-filter active noise control based on convolutional neural network, Signal Processing 190 (2022) 108317.

[10] S. M. Kuo, D. R. Morgan, Active noise control: a tutorial review, Proceedings of the IEEE 87 (6) (1999) 943–973.

[11] S. Elliott, Signal processing for active control, Elsevier, 2000.

[12] J. C. Burgess, Active adaptive sound control in a duct: A computer simulation, The Journal of the Acoustical Society of America 70 (3) (1981) 715–726.

[13] S. Elliott, I. Stothers, P. Nelson, A multiple error lms algorithm and its application to the active control of sound and vibration, IEEE Transactions on Acoustics, Speech, and Signal Processing 35 (10) (1987) 1423–1434.

[14] P. A. Nelson, H. Hamada, S. J. Elliott, et al., Adaptive inverse filters for stereophonic sound reproduction, IEEE Transactions on Signal Processing 40 (7) (1992) 1621–1632.

[15] P. A. Nelson, F. Orduña-Bustamante, H. Hamada, Multi-channel signal processing techniques in the reproduction of sound, in: Audio Engineering Society Conference: UK 7th Conference: Digital Signal Processing (DSP), Audio Engineering Society, 1992.

[16] S. U. Qureshi, Adaptive equalization, Proceedings of the IEEE 73 (9) (1985) 1349–1387.

[17] G. Malik, A. S. Sappal, Adaptive equalization algorithms: an overview, International Journal of Advanced Computer Science and Applications 2 (3) (2011).

[18] Y. Zhuang, Efficient filter design and implementation approaches for multi-channel constrained active sound control, Ph.D. thesis, Purdue University Graduate School (2023).

[19] Y. Zhuang, Y. Liu, An adaptive constrained multi-channel active noise control filter design approach using convex cone optimization, in: INTER-NOISE and NOISE-CON Congress and Conference Proceedings, Vol. 266, Institute of Noise Control Engineering, 2023, pp. 510–521.

[20] Y. Zhuang, Y. Liu, Constrained optimal filter design for multi-channel active noise control via convex optimization, The Journal of the Acoustical Society of America 150 (4) (2021) 2888–2899.

[21] S. J. Elliott, Optimal controllers and adaptive controllers for multichannel feedforward control of stochastic disturbances, IEEE Transactions on signal Processing 48 (4) (2000) 1053–1060.

[22] S. C. Douglas, A. Cichocki, S.-i. Amari, Self-whitening algorithms for adaptive equalization and deconvolution, IEEE Transactions on Signal processing 47 (4) (1999) 1161–1165.

[23] M. Bai, S. Elliott, Preconditioning multichannel adaptive filtering algorithms using evd-and svd-based signal prewhitening and system decoupling, Journal of sound and vibration 270 (4-5) (2004) 639–655.

[24] Y. Zhuang, Y. Liu, An efficient low-delay polyphase implementation method for active noise control systems, Applied Acoustics 227 (2025) 110232.

[25] D. Calvetti, L. Reichel, On the evaluation of polynomial coefficients, Numerical Algorithms 33 (2003) 153–161.

[26] G. A. Sitton, C. S. Burrus, J. W. Fox, S. Treitel, Factoring very-high-degree polynomials, IEEE Signal Processing Magazine 20 (6) (2003) 27–42.

[27] Y. Zhuang, Y. Liu, A stable IIR filter design approach for high-order active noise control applications, in: Acoustics, Vol. 5, MDPI, 2023, pp. 746–758.

[28] N. Wiener, Extrapolation, interpolation, and smoothing of stationary time series: with engineering applications, MIT press Cambridge, 1950.

[29] A. H. Sayed, T. Kailath, A survey of spectral factorization methods, Numerical linear algebra with applications 8 (6-7) (2001) 467–496.

[30] N. Wiener, P. Masani, The prediction theory of multivariate stochastic processes, Acta Mathematica 98 (1-4) (1957) 111–150.

[31] D. Youla, On the factorization of rational matrices, IRE Transactions on Information Theory 7 (3) (1961) 172–189.

[32] V. Kucera, Factorization of rational spectral matrices: a survey of methods, in: International Conference on Control 1991. Control'91, IET, 1991, pp. 1074–1078.

[33] G. Janashia, E. Lagvilava, L. Ephremidze, A new method of matrix spectral factorization, IEEE Transactions on information theory 57 (4) (2011) 2318–2326.

[34] Z. Wang, J. G. McWhirter, S. Weiss, Multichannel spectral factorization algorithm using polynomial matrix eigenvalue decomposition, in: 2015 49th Asilomar conference on signals, systems and computers, IEEE, 2015, pp. 1714–1718.

[35] J. G. McWhirter, P. D. Baxter, T. Cooper, S. Redif, J. Foster, An evd algorithm for para-hermitian polynomial matrices, IEEE Transactions on Signal Processing 55 (5) (2007) 2158–2169.

[36] T. Kailath, A. H. Sayed, B. Hassibi, Linear estimation, no. BOOK, Prentice Hall, 2000.

[37] H. Abou-Kandil, G. Freiling, V. Ionescu, G. Jank, Matrix Riccati equations in control and systems theory, Birkhäuser, 2012.

[38] R. E. Kalman, A New Approach to Linear Filtering and Prediction Problems, 2001, pp. 167–179. doi:10.1109/9780470544334.ch9.

[39] W. D. Stanley, G. R. Dougherty, R. Dougherty, H. Saunders, Digital signal processing (1988).

[40] M. Davis, Factoring the spectral matrix, IEEE Transactions on Automatic Control 8 (4) (1963) 296–305.

[41] A. J. Laub, Invariant subspace methods for the numerical solution of riccati equations, in: The Riccati Equation, Springer, 1991, pp. 163–196.

[42] Y. Zhuang, Y. Liu, A numerically stable constrained optimal filter design method for multichannel active noise control using dual conic formulation, The Journal of the Acoustical Society of America 152 (4) (2022) 2169–2182.

[43] F. Yang, Y. Cao, M. Wu, F. Albu, J. Yang, Frequency-domain filtered-x lms algorithms for active noise control: A review and new insights, Applied Sciences 8 (11) (2018) 2313.

[44] F. Albu, The constrained stability least mean square algorithm for active noise control, in: 2018 IEEE International Black Sea Conference on Communications and Networking (BlackSeaCom), IEEE, 2018, pp. 1–5.